Electric Potential and Field in Cylindrical Plasma Reactors with Helical Discharge Wires

M. Abdel-Salam
Electrical Engineering Department, Assiut University, Assiut, Egypt

ABSTRACT
This paper proposes for the first time a combined method based on boundary-elements and discrete-charge simulation for evaluating the electric potential and field in cylindrical reactors with helical discharge wire. This is a step forward for investigating the onset voltage of microdischarges and how they develop in these reactors. In the combined method, fictitious discrete point charges simulate the surface charge on the helical wire while surface-charged boundary elements represent the charge on the inner and outer surfaces of the glass tube. The effect of the wire diameter, the pitch of the helical wire as well as the thickness and relative-permittivity of the glass tube on the calculated field values are investigated.

1. INTRODUCTION
There are many sources that generate pollutants like SO_x, NO_x, CO_2, NH_3, CFC as well as fine dust particles. These include coal-burning plants, factories, internal combusion engines, animal farms and the like. SO_x, NO_x, air pollutants contribute to the acid rain. CO_2 pollutant contributes to the greenhouse effect which leads to abnormal heating of the atmosphere and can create a temperature inversion that traps pollutants. CFC pollutant contributes to the destruction of ozone layer in the upper atmosphere, thus the use of CFC will be limited in the world. City air may have an unacceptable level of SO_x, NO_x, and particles because of the heavy concentration of automobiles. Room air can be polluted by cigarette smoke which contains various poisonous gases including NH_3. Animal farms can also emit ammonia. It has unpleasant odor, unhygienic and should be removed together with other pollutants like SO_x, NO_x, etc.

The use of dc coronas for the removal of SO_x and NO_x from flue gas has been reported [1-3]. However, the process is energy inefficient and the performance is poor [4]. The poor performance is probably due to the small ionization region of dc coronas (small active treatment volume), and a large amount of energy is expended on ion migration which does not contribute to the production of radicals. The use of a pulsed streamer corona discharge avoids these difficulties. Streamers propagate across the entire gas treatment avoids these difficulties. Streamers propagate across the entire gas treatment-volume between electrodes, ionizing molecules and producing free electrons. This results in a larger active gas treatment-volume. The streamers leave positive ions which do not move significantly within their short period of the applied pulse with a subsequent improvement in power utilization efficiency.

Silent (dielectric-barrier) discharges in plasma reactors have been used for ozone generation in planar and cylindrical gemoetries [5]. In the planar geometry, one or both of the gap electrodes are covered with a thin dielectric layer, such as glass. In the cylindrical geometry, the discharge wire is stressed by AC voltage and the outer cylinder is a metal foil wrapped around a glass tube. The reactor plasma self-extinguishes when charge builds-up on the glass and reduces the local electric field near the discharge wire. Efficient chemical-processing based reactors for cleaning air from gaseous pollutants have been developed [6, 7] utilizing pulsed plasma (PPCP) and surface plasma (SPCP). The SPCP reactor generate every strong plasma in the reactor which is effective to decrease SO_x or NO_x. The PPCP with square-wave applied voltage showed effectiveness in decomposing CFC [8] and in NO_x removal [9] better than other AC discharge. With a helical discharge wire, the decomposition rate of CFC was higher [8] in comparison with a straight discharge wire extending along the axis of the of the cylindrical reactor. Moreover, helical discharge wire showed [10] higher yield ozone generation than straight wires.

Modeling of dielectric-barrier discharges in plasma reactors of planar geometries has received the attention of some investigators [11,12]. Modeling of dielectric-barrier discharges in cylindrical plasma reactors with a helical discharge wire has not yet been reported in the literature.

2. METHOD OF ANALYSIS
Figure 1a shows a schematic of the investigated cylindrical plasma reactors with a helical discharge wire touching the inner surface of the glass tube. The outer surface of the tube is wrapped by aluminum foil. The helical wire is of radius r_w, of pitch of τ and of N turns. The glass tube has inner radius r_g, thickness t, length L and relative permittivity ε_r.

The parametric equations which describe the coordinates (x_c, y_x, z_c) of any point on the axis of the discharge wire are expressed as:

$$\begin{aligned} x_c &= (r_g - r_w).\cos(\psi) \\ y_c &= (r_g - r_w).\sin(\psi) \\ z_c &= t.\psi / (2\pi) \end{aligned} \qquad (1)$$

where ψ is the angle defining the point on the wire-axis around the periphery of the tube. Fig. 1b.

2.1 Electric Potential and Field Calculation:
With the reactor stressed by an AC voltage, the surface charge on the helical wire as well as the charge on the inner and outer surfaces of the glass tube are not rotationally-symmetrical about factor axis. This represents a three-dimensional field problem and a combined technique based on boundary-elements and discrete-charge simulation is used for field calculation. Fictitious discrete point charges [13,14] are chosen to simulate the surface charge on helical wire while surface-charged boundary elements [15,16] are selected to represent the charge on the inner and outer surfaces of the glass tube.

2.2 Discrete-charges simulation technique applied to the helical wire:
The surface charges on each turn (pitch) of the helical wire are simulated by N_1 fictitious point charges distributed uniformly along the axis of the wire. The coordinates of each charge are expressed by eqn. (1) where ψ is incremented from a point charge to the next by angle $\Delta\psi = 2\pi/N_1$. Thus, the unknown point charges

simulating the helical wire as a whole are q_1, $i=1, 2, \ldots\ldots N$. N_1, where N is the number of turns of the helical wire.

2.3 Boundary-element simulation technique applied to the surfaces of the glass tube:

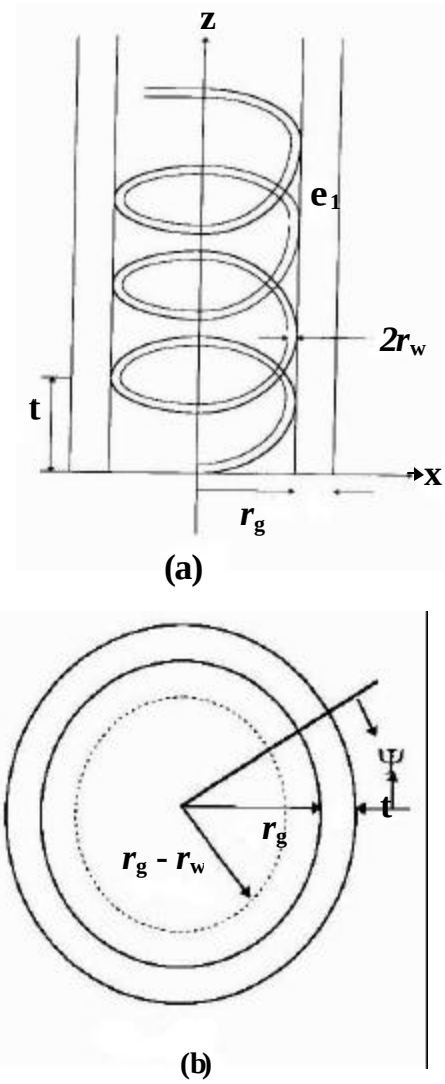

Fig. 1: The investigated reactor (a) Vertical cross-sectors (b) Horizontal plan view

The charge on each surface of the glass tube is simulated by N_e cylindrical elements in the ϕ-z coordinate system,

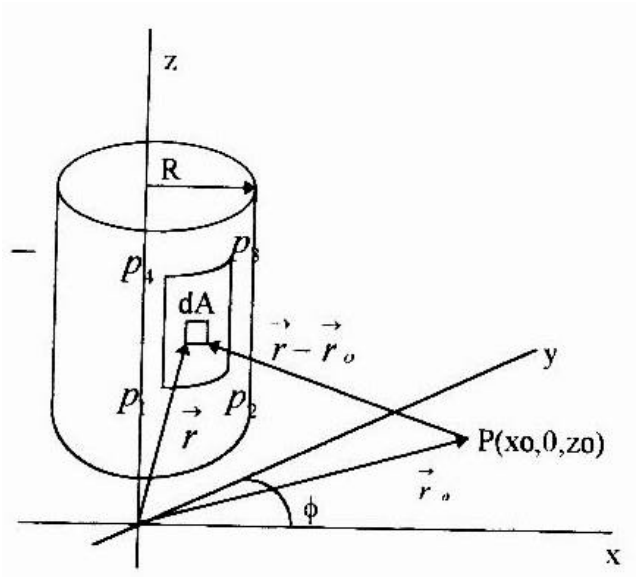

Fig. 2: A boundary element on the surface of the glass tube

Fig.2.

The charge density distribution in each element is expressed as:

$$\sigma = K_0 + K_1\phi + K_2 z + K_3 z\phi \qquad (2)$$

where K_0, K_1, K_2 and K_3 are coefficients related to the charge density values at the nodes of the elements. These elements form a grid on each surface of the glass tube where the face is divided into N_f and N_z divisions along the ϕ - and z- directions, respectively i.e. $N_e = N_f . N_z$ .The charge density σ_j, $j=1,2\ldots\ldots, N_f$. (N_z+1) is evaluated at the nodes of the grid whose number equals $N_f .(N_z+1)$. Thus, the total number of unknowns involved in the simulation of the surface charge of the two surfaces of the glass tube is $2N_f .(N_z+1)$. Therefore, the total number of unknowns involved in simulating the geometry as a whole (helical wire and glass tube) is $N.N_1+2N_f,. (N_z+1)$.

2.4 Potential equations:

The potential ϕ at any point $P(x_p, y_p, z_p)$ is the algebraic sum of potentials due to the point charges and surface–charged boundary elements simulating the wire and the glass tube:

$$\varphi(x_p, y_p, z_p) = \varphi_1(x_p, y_p, z_p) + \varphi_2(x_p, y_p, z_p) \qquad (3)$$

where φ_1 and φ_2 are respectively the contribution of the discrete point charge simulating the helical wire [13,14] and the boundary-element charges simulating the glass tube [15,16].

$$\varphi_1 = \frac{1}{4\pi\varepsilon_0}\cdot\sum_{i=1}^{NN_1}\frac{q_i}{\sqrt{(x_{c_i}-x_p)^2+(y_{c_i}-y_p)^2+(z_{c_i}-z_p)^2}} \qquad (4)$$

where x_{c_i}, y_{c_i} and z_{c_i} are the cartesian coordinates of the ith point charge as expressed by eqn. (1), ε_0 is the permittivity of free space.

$$\begin{aligned}\varphi_2 = \frac{1}{4\pi\varepsilon_0\Delta\phi\Delta z}\sum_{K=1}^{K=N_e}\{&\sigma_1.(z_2\phi_2.I_c - z_2.I_f - \phi_2.I_z + I_{zf})\\ &-\sigma_2.(z_2\phi_1.I_c - z_2.I_f - \phi_1.I_z + I_{zf})\\ &-\sigma_3.(z_1\phi_1.I_c - z_1.I_f - \phi_1.I_z + I_{zf})\\ &-\sigma_4.(z_1\phi_2.I_c - z_1.I_f - \phi_2.I_z + I_{zf})\}\end{aligned} \qquad (5)$$

where K stands for the element number, $(\phi_1,z_1),(\phi_2,z_1),(\phi_2,z_2)$, and (ϕ_1, z_2) are the coordinates of the nodes in the ϕ-z coordinate system belonging to the kth element on the surface of the glass tube.

$\Delta\phi$ and Δz represent the dimensions of the element $D\phi=2\pi/N_f$ and $Dz=L/N_f$ where L is the length of the glass tube in the z-direction.

I_c, I_z, I_f and I_{zf} are integral values expressed in terms of the coordinates of the nods of the kth element and coordinates (x_p, y_p, z_p) of the point P [15, 16].

To maintain the ground plane at zero potential, images of the charges simulating the rod and the barrier are taken into account.

2.5 Field equations:

The electric field $\vec{E}$ (of components E_x, E_y, E_z) at any point $P(x_p, y_p, z_p)$ is the vectorial sum of the fields due to the point charges and boundary elements simulating the helical wire and the glass tube;

$$\begin{aligned}\vec{E} = (x_p, y_p, z_p) &= (E_{x1}+E_{x2})\vec{a}_x + (E_{y1}+E_{y2})\vec{a}_y\\ &+ (E_{z1}+E_{z2})\vec{a}_z = E_x\vec{a}_x + E_y\vec{a}_y + E_z\vec{a}_z\end{aligned} \qquad (6)$$

with $\vec{a}_x$, $\vec{a}_y$ and $\vec{a}_z$ as unit vectors along the x,y- and z-axes.

The field components (E_{x1}, E_{y1}, E_{z1}) are those contributed by the point charges and obtained by differentiating the potential expressed by eqn. (4):

$$E_{x1} = \frac{1}{4\pi\varepsilon_0}.\sum_{i=1}^{N.N_1}\frac{x_p - x_{c_i}}{\sqrt{(x_p-x_{c_i})^2+(y_p-y_{c_i})^2+(z_p-z_{c_i})^2}}q_i \qquad (7a)$$

$$E_{y1} = \frac{1}{4\pi\varepsilon_0}.\sum_{i=1}^{N.N_1}\frac{x_p - x_{c_i}}{\sqrt{(x_p-x_{c_i})^2+(y_p-y_{c_i})^2+(z_p-z_{c_i})^2}}q_i \qquad (7b)$$

$$E_{z1} = \frac{1}{4\pi\varepsilon_0}.\sum_{i=1}^{N.N_1}\frac{x_p - x_{c_i}}{\sqrt{(x_p-x_{c_i})^2+(y_p-y_{c_i})^2+(z_p-z_{c_i})^2}}q_i \qquad (7c)$$

The field components (E_{x2}, E_{y2}, E_{z2}) are those contributed by the boundary-elements charges and obtained by differentiating the potential expressed by eqn. (6):

$$\begin{aligned}E_{x2} = \frac{-1}{4\pi\varepsilon_0\Delta\phi\Delta z}\sum_{K=1}^{K=N_e}[&\sigma_1(\phi_2 z_2 I_{cx} - \phi_2 I_{zx} - z_2 I_{fx} + I_{zfx})\\ &-\sigma_2(\phi_2 z_1 I_{cx} - \phi_2 I_{zx} - z_2 I_{fx} + I_{zfx})\\ &+\sigma_3(\phi_1 z_1 I_{cx} - \phi_1 I_{zx} - z_1 I_{fx} + I_{zfx})\\ &-\sigma_4(\phi_{21} z_1 I_{cx} - \phi_1 I_{zx} - z_2 I_{fx} + I_{zfx})]\end{aligned} \qquad (8a)$$

$$\begin{aligned}E_{y2} = \frac{-1}{4\pi\varepsilon_0\Delta\phi\Delta z}\sum_{K=1}^{K=N_e}[&\sigma_1(\phi_2 z_2 I_{cy} - \phi_2 I_{zy} - z_2 I_{fy} + I_{zfy})\\ &-\sigma_2(\phi_2 z_1 I_{cy} - \phi_2 I_{zy} - z_2 I_{fy} + I_{zfy})\\ &+\sigma_3(\phi_1 z_1 I_{cy} - \phi_1 I_{zy} - z_1 I_{fy} + I_{zfy})\\ &-\sigma_4(\phi_{21} z_1 I_{cy} - \phi_1 I_{zy} - z_2 I_{fy} + I_{zfy})]\end{aligned} \qquad (8b)$$

$$\begin{aligned}E_{z2} = \frac{-1}{4\pi\varepsilon_0\Delta\phi\Delta z}\sum_{K=1}^{K=N_e}[&\sigma_1(\phi_2 z_2 I_{cz} - \phi_2 I_{zz} - z_2 I_{fz} + I_{zfz})\\ &-\sigma_2(\phi_2 z_1 I_{cz} - \phi_2 I_{zz} - z_2 I_{fz} + I_{zfz})\\ &+\sigma_3(\phi_1 z_1 I_{cz} - \phi_1 I_{zz} - z_1 I_{fz} + I_{zfz})\\ &-\sigma_4(\phi_{21} z_1 I_{cz} - \phi_1 I_{zz} - z_2 I_{fz} + I_{zfz})]\end{aligned} \qquad (8c)$$

where I_{cx}, I_{cy} and I_{cz} are respectively $\frac{\partial I_c}{\partial x}$, $\frac{\partial I_c}{\partial y}$ and $\frac{\partial I_c}{\partial z}$;

I_{zx}, I_{zy} and I_{zz} are respectively $\frac{\partial I_z}{\partial x}$, $\frac{\partial I_z}{\partial y}$ and $\frac{\partial I_z}{\partial z}$;

I_{fx}, I_{fy} and I_{fz} are respectively $\frac{\partial I_f}{\partial x}$, $\frac{\partial I_f}{\partial y}$ and $\frac{\partial I_f}{\partial z}$;

I_{zfx}, I_{zfy} and I_{zfz} are respectively $\frac{\partial I_{zf}}{\partial x}$, $\frac{\partial I_{zf}}{\partial y}$ and $\frac{\partial I_{zf}}{\partial z}$.

2.6 Boundary conditions:

The boundary conditions are Dirichlet condition at the helical wire and the outer surface of the glass tube.

The calculated potential is equal to the applied voltage V at the surface of the helical wire (where the aluminum foil is wrapped and grounded), i.e.

$$\varphi = V \qquad (9)$$

At the inner surface of the glass tube, the Neumonn condition, where the continuity of the normal electric flux density in (the r-direction) is satisfied, i.e.

$$\varepsilon_r E_{rd} = E_{ra} \qquad (10)$$

where E_{rd} and E_{ra} are the r-components of the electric field calculated at any point on the inner surface of the

glass surface when seen from the dielectric and air sides respectively;

$$E_{rd} = E_r - \frac{\sigma}{2\varepsilon_0} \quad ; \quad E_{ra} = E_r + \frac{\sigma}{2\varepsilon_0}$$

$$E_r = \sqrt{E_x^2 + E_y^2}$$

where σ is the value of the surface charge density at the point and is evaluated by eqn. (2).

At the outer surface of the glass tube where the aluminum foil is wrapped;

$$\phi = 0.0 \qquad (11)$$

2.7 Boundary points:

The satisfy the boundary conditions, boundary points are chosen on the helical wire as well as the surface of the glass tube.

Corresponding to each point charge simulating the surface charge on the helical wire ($r_g - 2r_w$), a boundary point is chosen with coordinates.

$$x_c = (r_g - 2r_w).\cos(\gamma)$$
$$y_c = (r_g - 2r_w).\sin(\gamma) \qquad (12)$$
$$z_c = t.\gamma/(2\pi)$$

On each surface of the glass tube, the boundary points are chosen uniformly distributed in the ϕ- and z- directions with a number equal to that of the nodes [$=N_f.(N_z + 1)$] where the charge density values are to be evaluated.

2.8 Determination of the unknowns:

With the aid of eqns. (3) and (6) for the potential and field, the boundary conditions expressed by eqns. (9) through (11) are satisfied at the boundary points chosen on the helical wire and the glass tube. This results in a set of [$=N.N_1 + 2(N_z + 1).N_f$] simultaneous equations whose solution determines the values of the unknowns; (q^s), the values of the point charges and (s^s), the charge-density values at the nodes on both surfaces faces of the glass tube.

3. NUMERICAL DATA

The helical wire of the investigated cylindrical plasma reactor (base case) has a radius r_w of 0.5 mm, pitch τ of 10mm and number of turns N of 10. The glass tube has inner radius r_g of =10mm, thickness t of 1 mm and relative-permittivity ε_r of 3. The wire radius is increased to 0.75 mm, the pitch is increased to 16.667 mm and the relative permittivity is increased to 6. The thickness of the glass tube is increased to 2 mm. The length L of the glass tube is 100 mm and remains constant. Thus, the number of turns N is decreased from 10 (pitch = 10mm) to 6 (pitch = 16.667 mm). The number of point charges N_1 per turn of the helical wire is chosen 90. The number of divisions N_ϕ and N_z for the inner and outer surfaces of the glass tube are chosen 17 and 17. Thus, the number of unknown point charges simulating a 10-tum helical wire is 900 and the number of unknowns involved in the simulation of the inner and outer surfaces of the glass tube is 612. Thus, the total number of unknowns involved in simulating the reactor as a whole is 1512. This resulted in a deviation of the calculated potential by less than 0.1% of the voltage applied to the helical wire at check points selected between the boundary points on the wire. Moreover, the Neumann boundary condition is satisfied within an error not more that 1% at check points selected away from where the helical wire touches the inner surface of the glass tube. At the touch points which represent triple-junction points the electric field is excessively high and could not be evaluated numerically [17,18].

In a related study,the effect of the surface charges on the side faces of a vertical barrier located nearby to a rod-gap was found negligible and the electric field values on the gap axis did not increase by more than 0.3% of their values when considering only the front and rear faces of the barrier [19]. In the present study, the thickness of the glass tube is small to the extent to consider only the charges on the inner and outer surfaces of the glass tube.

4. RESULTS AND DISCUSSION

As the pitch of the helical wire decreases, the potential and field along the reactor axis increases, Figs. 2 and 3. For the same pitch, the potential is small at the reactor ends and increases towards the center of reactor, Fig. 2. The increase is fast at first followed almost by a constant potential along the reactor axis. The electric field along the reactor axis, being equal to the potential derivative, is high at the reactor ends, Fig. 3. All of this is attributed to the end effect of the reactor.

In the mid-plane of the reactor, the field is maximum at the discharge-wire surface and decreases towards the center of the reactor. The field across the reactor diameter increases with the permittivity of the glass tube, Fig. 4, in conformity with Neumann condition. The field also increases with the diameter of the discharge wire, Fig. 5. However, the field decreases with the increase of the thickness of the glass tube, Fig. 6. This is explained by the field enhancement due to the charge on the outer surface of the glass tube. Such enhancement decreases with the increase of tube thickness.

5. CONCLUSIONS:

1. A combined method based on boundary-elements and discrete-charge simulation for evaluating the electric potential and field in cylindrical reactors with helical discharge wire is proposed.
2. For the same pitch, the potential is small at the reactor ends and increases towards the center of reactor.
3. For the same pitch, the electric field along the reactor axis, being equal to the potential derivative, is high at the reactor ends.
4. The field across the reactor diameter is maximum at the discharge-wire surface and decreases towards the center of the reactor.
5. The field across the reactor diameter increases with the permittivity of the glass tube, Fig. 4 and the diameter of the discharge wire.
6. The field across the reactor diameter decreases with the increase of the thickness of the glass tube.

6. ACKNOWLEDGEMENT

The author wishes to acknowledge Prof. Dr.-Ing. H. Singer and Dipl.-Ing. A. Ahmed of the Technical University of Hamburg-Harburg, Germany for their fruitful discussions during the progress of the present computations using the boundary element method.

7. REFERENCES

[I] J. S. Chang, in Non-Thermal Plasma Techniques for Pollution Control, B. Penetronte Ed., Plenum Press, New York, 1993.

[2] A. Mizuno, A. Chakrabarti and K Okazaki, Advanced Research Workshop on Non-Thermal Plasma Techniques for Pollution Control, Cambridge England, Sept 1992.

[3] L. Civitano and E Sani, Plasma Technology, M Capitelli and C. Gorse, Eds., Plenum Press, New York, 1992.
[4] A. Mizuno, J. S. Clements and R. H. Davis, Proc. IEEE Industry Applications Society Conf., pp. 1015-1020, 1984.
[5] B. M. Penetrante, " Non-Thermal Plasma Techniques for Pollution Control", Pt. A, eds. B.M. Penetrante and S. E. Schultheis, Springer-Verlag, Germany, 1992.
[6] S. Masuda, S, Hosokawa, X. Tu and Z. Wang, Proc. 5th Int. Con. on Electrostatic Precipitation, Washington DC., USA, April 5-8, 1093.
[7] S. Masuda, Proc. EPR/NSF Symp. on Environmental Applications of Advanced Oxcidation Technologies, San Francisco, USA, Feb 22-24, 1993.
[8] T. Oda, R. Yamashita, T. Takahashi and S. Masuda, Proc. IEEE Industry Applications Society Conference, Toronto, Canda, pp. 1983-1988, 1993.
[9] A. Mizuno, K. Shimizu, A. Chakrabarti, L. Dascalescu and S. Furuta, Proc. IEEE Industry Applications Society Conference, pp. 1977-1982, 1993.
[10] Castle, et al., Proc. IEEE Industry Applications Society Conference, pp. 1111-1118, 1993.
[11] D. Braun, U. Küchler and G. Pietsch, J. Phy. D: Appl. Phys., Vol. 24, pp. 564-572, 1991.
[12] B. Eliasson, M. Hirth and U, Kogeischatz, J. Phys. D.: Appl. Phys., Vol. 20, pp. 1421-1437, 1987.
[13] H. Singer, H. Steinbigier and P. Weiss, IEEE Trans. on Power App. & Sys. , Vol. 93, pp, 1660-1668, 1974.
[14] M. Abdel-Salam, et al., "Electric Fields" in "High Voltage Engineering Theory and Practice", Marcel Dekker, Inc., New York, USA, 2000.
[15] F. Gutfleisch, H. Singer, K. Forger and J. A. Gomollon, IEEE Trans. on Power Delivery, Vol.9, pp. 743-749, 1994.
[16] F. Gutfleisch, Dr.-Ing. Thesis, Technical University of Hamburg-Harburg, 1989.
[17] P. Weiß, Proc. 3rd ISH, Milan, Italy, Aug. 1979, paper No 11-21.
[18] K. J. Murtz and P Weiß, Proc. 7th Int. Conf. on Gas Discharges and Their Applications", London, England, pp. 478-48 1, Aug./Sept. 1982.
[19] M. Abdel-Salam, H. Singer and A. Ahmed, J. Phy. D: Appl, Phys., Vol. 30, pp. 1017-1028, 1997.

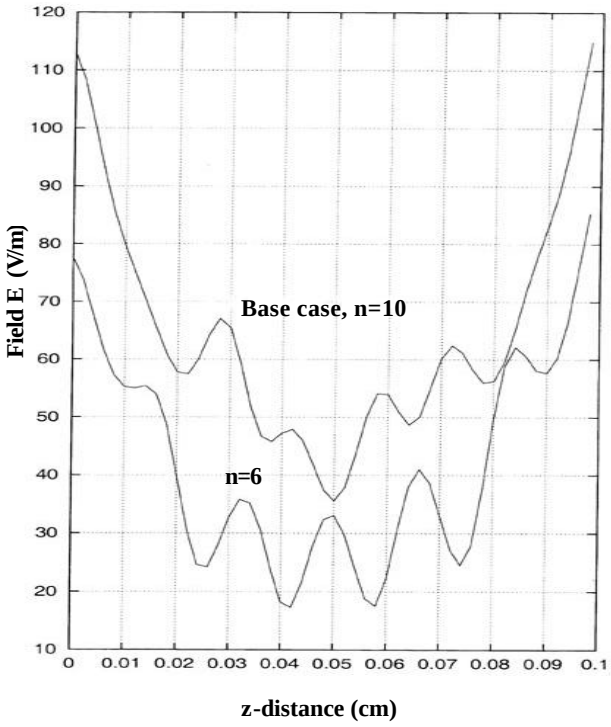

Fig. 4: Change of the electric field along the reactor diameter axis as influenced by the pitch of the helical wire.

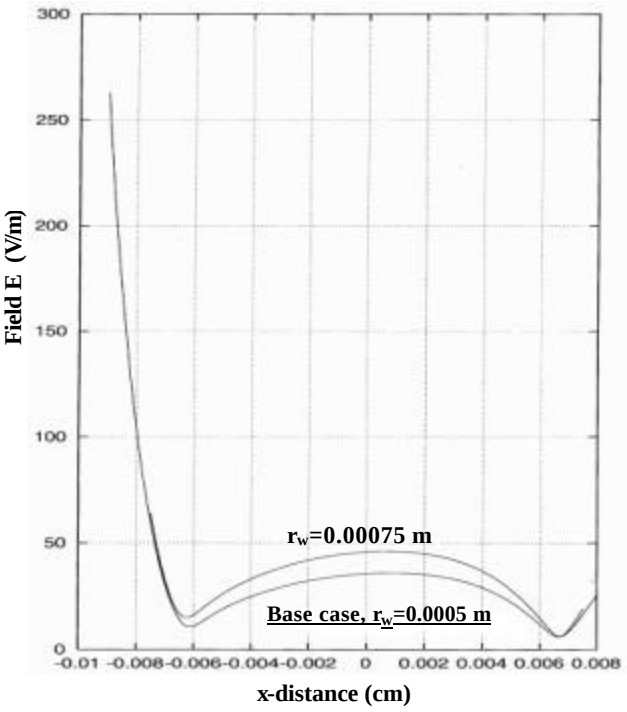

Fig. 6: Change of the electric field along the reactor diameter axis as influenced by the pitch of the helical wire.